RESEARCH ARTICLE | FEBRUARY 25 2026

Sequence-encoded patterning of stickers modulates biomolecular condensate reconfiguration in IDP systems FREE

Special Collection: Yijing Yan Festschrift

Xubiao Ji ; Zhonghuai Hou

J. Chem. Phys. 164, 085103 (2026)
https://doi.org/10.1063/5.0323902

The Journal of Chemical Physics ARTICLE pubs.aip.org/aip/jcp

Sequence-encoded patterning of stickers modulates biomolecular condensate reconfiguration in IDP systems

Cite as: J. Chem. Phys. 164, 085103 (2026); doi: 10.1063/5.0323902
Submitted: 21 January 2026 • Accepted: 7 February 2026 •
Published Online: 25 February 2026

Xubiao Ji and Zhonghuai Hou[a)]

AFFILIATIONS

Hefei National Research Center for Physical Sciences at the Microscale, Department of Chemical Physics, University of Science and Technology of China, Hefei, Anhui 230026, China

Note: This paper is part of the Special Topic, Yijing Yan Festschrift.
[a)]**Author to whom correspondence should be addressed:** hzhlj@ustc.edu.cn

ABSTRACT

Intrinsically disordered proteins (IDPs) exert pivotal roles in Phase Separation Coupled to Percolation (PSCP), a process that drives the formation of functional biomolecular condensates linked to diverse cellular physiological activities. In this study, we investigate how sequence-encoded mesoscopic patterning modulates PSCP in IDP systems by leveraging the classic stickers-and-spacers framework, combined with coarse-grained molecular dynamics simulations. Intriguingly, our analysis demonstrates that the distribution of stickers plays important roles: compactness of sticker arrangement on IDPs exerts a substantial influence on IDP clustering process, while the patterning heterogeneity of the arrangement additionally impacts the morphology of the resulting aggregations. Subsequent findings elucidate that sparse and homogeneous stickers facilitate the emergence of robust aggregation, whereas proximal sequential organization directly induces dispersed and small clusters. These discoveries are validated through the statistical quantification of void volume fraction ϕ_{void} (serving as a referential measure for condensate maturation) in conjunction with the quantification of the total stickers present on the cluster surfaces. Collectively, this work may shed new lights on the underlying mechanism for regulating IDP-mediated phase separation.

INTRODUCTION

It is widely recognized that phase separation is a prevalent physiological phenomenon in cells;[1–4] among these processes, Phase Separation Coupled to Percolation (PSCP), a phase transition process defined by synergistic density and connectivity transitions, is particularly relevant to the sticker–spacer intrinsically disordered protein (IDP) systems investigated herein.[5,6] The formation of numerous membraneless organelles or condensates is associated with such phase separation processes involving biomolecules.[7–9] These condensates play critical roles in organizing biochemical processes, facilitating essential functions, such as transcriptional regulation,[10,11] stress responses,[12,13] and the assembly of signaling complexes,[14] allowing for the compartmentalization of cellular activities without the need for membrane-bound structures.[15–18]

Recent experimental studies have increasingly demonstrated that intrinsically disordered proteins (IDPs),[19–23] which constitute a significant class of biomolecules that challenge the traditional structure–function paradigm in protein science, also play a crucial and irreplaceable role in driving PSCP within organisms.[24–27] In contrast to folded proteins,[28–30] IDPs exhibit exceptional conformational flexibility and do not adopt a stable three-dimensional architecture under physiological conditions.[31–34] Owing to their intrinsic disorder, IDPs possess a distinctive capacity for molecular interactions—an ability that is essential for driving the density changes (via cluster assembly or disassembly) and connectivity transitions (via inter-cluster association or void network formation) that underpin PSCP. This capacity further supports a broad spectrum of cellular functions, including signaling, regulation, and cellular organization.[35–39] Disruptions in the PSCP of IDPs have been implicated in several neurodegenerative disorders,[38,40–42] highlighting the importance of understanding the mechanisms underlying this phenomenon.

Generally, IDPs feature a dual-module architecture, one comprising regions with pronounced interactions and the other consisting of regions devoid of significant interactions, the latter

serving predominantly as a connector.[43–46] A distinctive approach in contemporary coarse-grained hierarchical simulations examining the phase separation behavior of IDPs involves modeling the significantly interacting modules within the IDP sequence as "stickers," while the primarily connective segments are designated as "spacers."[47–51] This methodology is crucial for accurately capturing the fundamental properties inherent to the structural sequence of IDPs. Importantly, emerging evidence emphasizes that the linear patterning of substantial interaction motifs along IDP sequences determines their phase separation behavior. For instance, site-directed mutagenesis targeting aromatic residues (Tyr/Phe) in the intrinsically disordered regions (IDRs) of Ddx4 and BugZ was found to restrict phase separation behavior;[52,53] moreover, the mutation of Tyr residues in an IDR of hnRNPA2 inhibited the formation of phase-separated droplets.[54] The measured saturation concentrations across all twelve constructs collectively exhibited an inversely proportional relationship with the product of tyrosine and arginine sticker residue counts yet display structural-concentration divergences even when their sticker–product values are identical.[55] These findings underscore that IDP phase behavior depends not merely on the interaction valency and strength, concepts central to hierarchical models that account for both strong sticker–sticker and weak spacer–spacer interactions,[56] but is also exquisitely regulated by their linear patterning along the sequence. This offers a design principle for engineering biomaterials and targeting PSCP-associated disorders. While the importance of sequence features is recognized, the qualitative rules governing how the one-dimensional patterning of stickers, specifically the statistical characteristics of inter-sticker spacing, determines condensate architecture remain to be fully characterized.

To contend with this issue, we deploy the stickers-and-spacers modeling framework. While it is now appreciated that spacers can contribute non-specific interactions and modulate phase behavior,[56] we employ a reductionist model where spacers are treated as inert, repulsive segments. This deliberate simplification is essential to isolate the specific, causal impact of one-dimensional sticker patterning from the confounding effects of spacer properties. Through this approach, we reveal that the sequence patterning of stickers in IDPs crucially dictates their phase-separation behavior. The sequence architecture is mainly characterized by two parameters: the mean distance λ between adjacent stickers and the variance ξ of these distances. These metrics respectively quantify the intrachain sticker compaction and the distribution heterogeneity of the stickers. Our extensive simulations demonstrate that the degree of local sticker clustering dictates the size of the aggregate clusters, while the heterogeneity in inter-sticker spacing further influences the morphology of the condensates. Further systematic analysis has revealed that robust clustering predominantly occurs in IDPs characterized by a sparse and homogeneous distribution of stickers, whereas a dense distribution of stickers directly fosters the formation of small and dispersed clusters, as validated by the statistical analysis of the void volume fraction that serves as a referential measure for clustering participation and the quantification of the total stickers present on the cluster surfaces. These findings may provide essential theoretical insights for modulating IDP phase separation, with potential implications for addressing neurodegenerative diseases linked to IDP aggregation.

MODELS AND METHODS

We consider a system composed of n_I IDPs, each with the coarse-grained stickers-and-spacers model of IDP, which is schematically illustrated in Fig. 1. Under the framework of this modeling, the strongly interacting modules within IDP sequences are coarse-grained as spherical "stickers" (represented by blue spheres) with characteristic diameter σ_c and mass m_c, while the predominantly non-interacting linker segments are modeled as "spacers" (depicted by red spheres) with diameter σ_p and mass m_p. The simulated system comprises n_I independent IDP chains, each containing a fixed total of n_c stickers and n_p spacers. This study specifically investigates how the linear arrangement of stickers along the polymer backbone influences phase separation behavior, while maintaining constant total sticker content.

To characterize the distribution patterns of these stickers along the IDP, we define the inter-sticker spacing distance x ($1 \le x \le 20$), and the distribution pattern is described by two key parameters: the mean spacing λ and variance $\xi = \sigma^2$ of x, to quantify the compactness and heterogeneity of the sticker distribution. Although the theoretical maximum inter-sticker spacing could exceed 20, excessively large spacing values would lead to extremely heterogeneous spacer allocation across different sticker pairs. This heterogeneity would result in a drastic increase in the variance of inter-sticker spacing, making it impossible to stably reproduce the predefined target variance values that are critical for our comparative analysis. It is crucial to note that conformational degeneracy persists even under fixed parameters (λ, ξ) quantifying sticker sequence distribution. In our simulations, all IDP chains in our simulation system do not share an identical sequence; instead, each chain is stochastically generated under the constraint that the mean and variance of its inter-sticker spacing conform to the predefined parametric values. In other words, any IDP chain sequence that satisfies the target statistical characteristics of sticker spacing was included in the system, leading to a library of diverse sequences rather than a homogeneous set of identical chains. Furthermore, in addition to the sequence heterogeneity, the initial three-dimensional conformations of these 2000 chains were also randomly assigned. Collectively, this dual randomization (sequence and initial conformation)

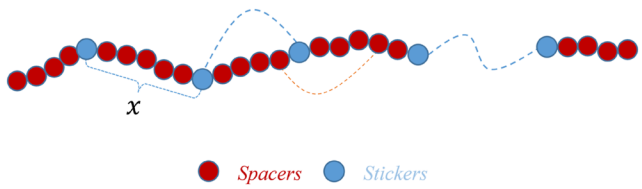

FIG. 1. The coarse-grained stickers-and-spacers model for IDPs employs an idealized representation where strongly interacting domains within IDPs are mapped as spherical stickers (blue spheres) with diameter σ_c and mass m_c, while the predominantly non-interacting linker segments are modeled as spherical spacers (red spheres) with diameter σ_p and mass m_p. The simulation contains n_I independent IDP chains, each comprising a fixed total of n_c stickers and n_p spacers arranged in sequence. To characterize the distribution patterns of these stickers along the IDP, we define the inter-sticker spacing distance x ($1 \le x \le 20$), and the distribution pattern is described by two key parameters: the mean spacing λ and variance $\xi = \sigma^2$, to quantify the compactness and heterogeneity of the sticker distribution.

constructs a heterogeneous conformational ensemble, which better mimics the intrinsic diversity of natural IDP systems, rather than a homogeneous system with identical sequences and conformations. For each combination of λ and ξ, we performed five fully independent simulations. The key details of these independent runs are as follows: Each replicate was initialized with distinct, uncorrelated starting states, including random spatial distributions of the 2000 coarse-grained chains (each comprising 100 beads) and random initial conformations of individual chains. No overlap or correlation existed between the initial configurations of different simulations, ensuring the independence and statistical validity of each replicate. The intrachain bonded interactions in IDPs are modeled through harmonic spring potentials $U_b(r_{ij}) = K_b(r_{ij} - r_0)^2$, wherein r_{ij} denotes the distance between the corresponding ith and jth units and K_b represents the spring constant. Inter-sticker nonbonded interactions are described by an attractive Lennard-Jones (LJ) potential $U_{cc}(r_{ij}) = 4\epsilon_{cc}\left[(\sigma_{cc}/r_{ij})^{12} - (\sigma_{cc}/r_{ij})^{6}\right]$, wherein ϵ and σ here and after denote the LJ well depth and zero-potential distance, respectively. The sticker–spacer and spacer–spacer interactions are governed by the purely repulsive Weeks–Chandler–Andersen (WCA) potential $U_{\alpha\beta}(r_{ij}) = 4\epsilon_{\alpha\beta}\left[\left(\sigma_{\alpha\beta}/r_{ij}\right)^{12} - \left(\sigma_{\alpha\beta}/r_{ij}\right)^{6}\right] + \epsilon_{\alpha\beta}$ for $r_{ij} \le \sqrt[6]{2}\sigma_{\alpha\beta}$ and $U_{\alpha\beta}(r_{ij}) = 0$ otherwise, wherein $\alpha\beta = cp\ or\ pp$. It is important to state that our treatment of spacers as purely repulsive is a deliberate reductionist choice and a specific theoretical construct of this model. This approach is not intended to negate the established understanding that spacers in real IDP systems can contribute weak, non-specific interactions and modulate phase behavior. In contrast, by defining spacers as inert, we aim to isolate the specific, causal impact of one-dimensional sticker patterning on cluster architecture, systematically eliminating the confounding effects of spacer properties. The insights gained from this well-defined baseline are crucial for deconvoluting the complex drivers of phase separation. To streamline the computational framework, our CG model employs LJ and WCA potentials not as literal representations of specific interactions (e.g., hydrophobic, cation-π, and H-bonding) but as effective potentials that collectively capture the net thermodynamic consequences of these underlying chemistries in driving phase separation. The LJ attraction term implicitly integrates the cohesive effects arising from hydrophobic burial, weak van der Waals forces, and transient non-specific attractions. Conversely, the WCA repulsion encodes steric exclusion and charge repulsion (at short ranges).

The diameter of spacers σ_p, the interaction strength between two different spacers ϵ_{pp}, and the mass of spacers m_p are chosen as basic units. Other parameters are set as follows: $n_I = 2000$, $n_c = 20$, $n_p = 80$, $K_b = 100$, $r_0 = 1.0$, $\sigma_c = 1$, $m_c = 1$, $\epsilon_{pc} = 1.0$, $\epsilon_{cc} = 2.5$, $\sigma_{cc} = \frac{\sigma_c+\sigma_c}{2} = 1.0$, $\sigma_{cp} = \frac{\sigma_c+\sigma_p}{2} = 1.0$, and $\sigma_{pp} = \frac{\sigma_p+\sigma_p}{2} = 1.0$. Molecular dynamics simulations were performed using the LAMMPS package on systems containing IDP chains with sticker distributions characterized by two parameters λ and ξ in a $220 \times 220 \times 220$ box with periodic boundary conditions. The Nose–Hoover hot bath of temperature $T = 1.0$ is adopted to ensure NVT ensemble sampling. The integration time step was set to $\delta t = 0.01$, and 10^6 steps are used for equilibration. Dynamic variables are averaged over 2×10^5 steps in the equilibrium state, and all the snapshots shown below are recorded at time.

RESULTS AND DISCUSSION

To elucidate the role of sticker linear patterning in governing IDP phase separation behaviors, Fig. 2 presents the characteristic simulation snapshots for two extremal configurations: optimally uniform distribution ($\xi = 0$) and most sparsely packed arrangement ($\lambda = 5$). It is unequivocally evident that the alterations in the λ parameter exert a profound influence on cluster growth, with the maximum cluster size exhibiting a positive correlation with variations in λ. In other words, the alignment of stickers within the sequence exerts a considerable influence on modulating the clustering of IDPs; in particular, a sparse arrangement enhances the phase separation propensity of IDPs when stickers are evenly distributed. Moreover, we also explore the impact of distributional heterogeneity on IDPs' phase separation behavior, while maintaining a fixed mean spacing ($\lambda = 5$) for the sticker distribution. It is apparent that

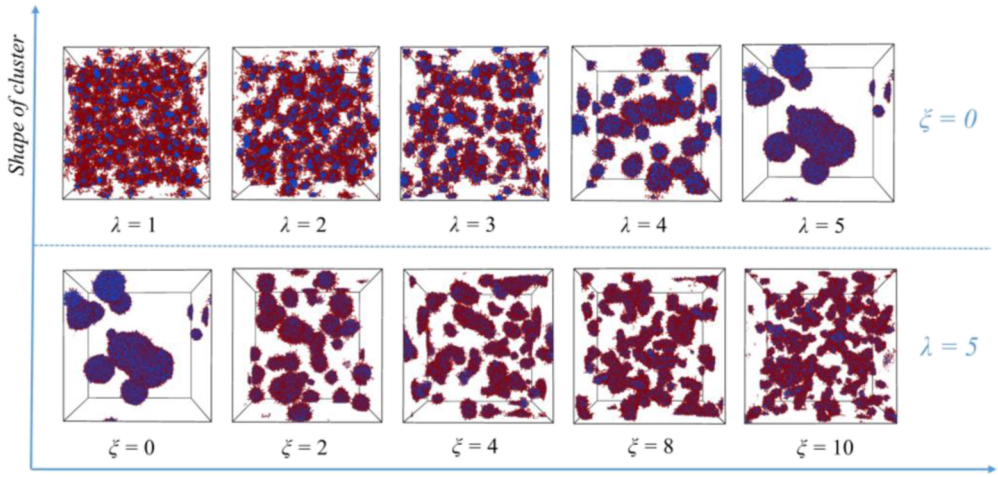

FIG. 2. Typical snapshots of IDPs featuring stickers arranged under varying conditions encompassing different distribution patterns, when stickers are optimally uniformly distributed $\xi = 0$ and most sparsely packed $\lambda = 5$.

the distributional heterogeneity significantly alters the cluster morphology for the sparsest configuration. Collectively, these results underscore the pivotal role of the arrangement of stickers on the IDP chain in governing both the clustering behavior and morphological characteristics of IDP phase separation.

To facilitate a comprehensive comparison of the simulated snapshots across various patterning scenarios, we meticulously aggregated and integrated the simulated snapshots from diverse distribution cases to construct a holistic overview, as illustrated in Fig. 3. For the rare cases where the distribution does not meet the specific variance value, we adopt the arrangement most closely approximating the selected variance as a substitute; this approach still physically represents the degree of heterogeneity in the spacing of the sticker distribution. It is evident that the phase separation behavior of IDPs undergoes pronounced alterations in accordance with the variations in the λ value that parameterizes the sequence; in particular, an elevation in the λ value of invariably facilitates the emergence of larger clusters, even when the variance remains constant. Notably, the ξ value associated with stickers' distribution exerts negligible influence when the λ value is minimal, while it substantially affects both its clustering and morphological characteristics when the λ value is elevated. It is crucial to emphasize that an intensification of the distributional heterogeneity of stickers appears to induce an increasingly pronounced deviation from

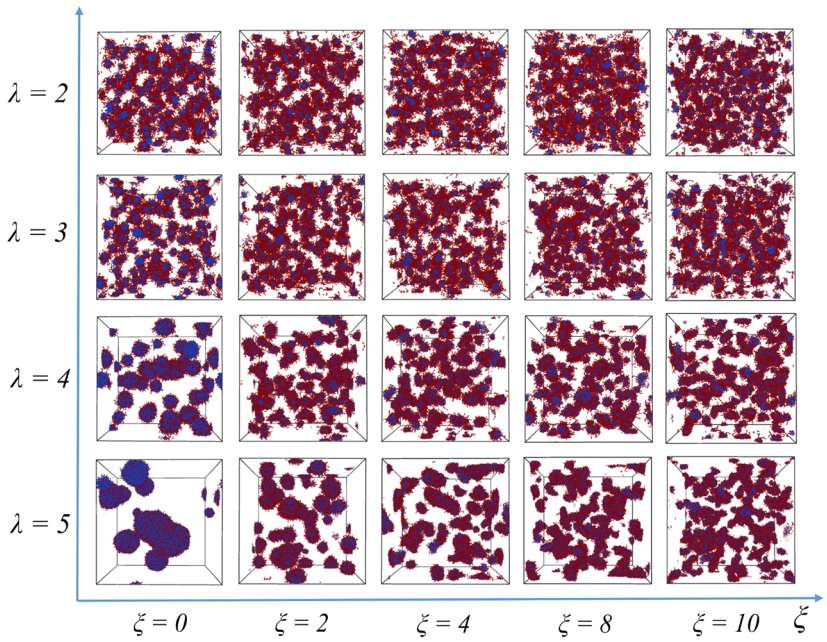

FIG. 3. Representative simulation snapshots under different configurations, which are strategically selected across distinct parameter values of ξ and λ; for the rare cases where the distribution does not meet the specific variance value, we adopt the arrangement most closely approximating the selected variance as a substitute. This approach still physically represents the degree of heterogeneity in the spacing of the sticker distribution.

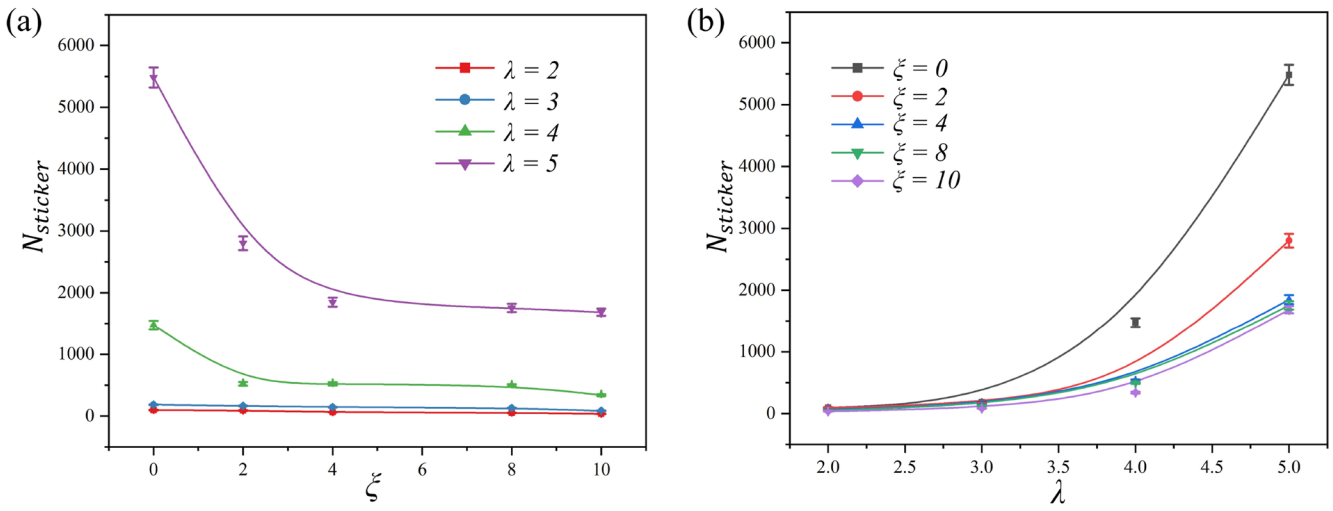

FIG. 4. Statistical values of sticker quantities on cluster surfaces varying as functions of parameters (a) ξ and (b) λ, respectively.

spherical symmetry, with the clusters becoming progressively more distorted and asymmetric.

Given the pronounced interactional characteristics of stickers along the IDP chain, a more profound comprehension of the substantial disparity in cluster sizes and morphologies induced by divergent sticker arrangement sequences necessitates a meticulous quantification of the total stickers present on the cluster surfaces, as illustrated in Figs. 4(a) and 4(b). Crucially, the influence of ξ becomes markedly significant in modulating the distribution of surface stickers when λ is large. In particular, the presence of several stickers in close proximity within the IDP chain induces a configuration where the majority of IDPs align head-to-head at the cluster core, while the cluster surfaces are predominantly occupied by spacers that exhibit negligible interactional effects. This arrangement fosters a more dispersed, less cohesive clustering structure rather than the formation of a singular, dominant aggregate, and this finding is in consonance with those snapshots depicted in Fig. 2. Moreover, when λ is small, the effect of ξ is negligible on the total number of surface stickers, corroborating the minimal morphological changes observed in Fig. 3 under the same conditions. In addition, Fig. 4(b) underscores that the variations in λ exert an undeniable influence on the distribution of surface stickers when the ξ value is fixed, particularly for $\xi = 0$. The statistical analysis of surface sticker distributions reveals the underlying clustering tendencies, which are consistent with the morphological trends observed previously.

In order to accurately quantify the degree of phase separation within the sticker arrangement sequence, we meticulously analyzed the volume fraction of voids under the specified conditions. In particular, we employed a unit-based scanning method using a cubic unit cell, ensuring an unambiguous classification of particle-occupied and unoccupied regions, to systematically analyze the entire domain of each scenario presented in Fig. 3. The box is partitioned into non-overlapping $20 \times 20 \times 20$ lattice-unit small grids, which are scanned sequentially. Each grid is labeled "occupied" if occupied by particles, or "void" if empty. In 3D space, void grids are defined as "connected" only via face-sharing adjacency; those contacting solely through edges or vertices are excluded from connected void clusters to avoid the overestimation of void connectivity. The total void volume fraction is the ratio of all void grids to the total grid count, while the maximum void volume fraction refers to the ratio of grids in the largest connected void cluster to the total grid count. Utilizing the smallest void as a fundamental unit, designated as $20 \times 20 \times 20$, we computed the corresponding max and total void volume fractions for each scenario depicted in Fig. 3, as presented in Figs. 5(a) and 5(b).

These metrics can be employed as an order parameter to indirectly assess the extent of IDPs' involvement in the phase separation process. Our grid-based approach is tailored to our system's focus on cluster–void coexistence, and it provides an indirectly, macroscopically representative measure of the density transition in PSCP. In particular, the total void volume fraction quantifies the overall separation between dense (cluster) and dilute (void) phases: a higher total void volume fraction indicates more pronounced density partitioning between clusters and the bulk. The maximum void volume fraction we reported is inherently a connectivity metric: a larger maximum void volume fraction indicates that unoccupied regions are highly interconnected, which corresponds to more aggregated clusters and stronger system-level connectivity; conversely, a smaller maximum void volume fraction reflects fragmented clusters and weaker connectivity. In particular, when protein clusters are highly dispersed, occupied grids distribute uniformly and widely across the system, leading to several isolated small voids and, thus, smaller total and maximum void volume fractions. In contrast, when large aggregated clusters form, occupied grids concentrate in localized regions, allowing adjacent void grids to merge into large connected domains, which results in larger total and maximum void volume fractions and better void connectivity.

Notably, as depicted in Fig. 5, when the variance is fixed, an increase in the λ value (which signifies a more sparse distribution) corresponds to a significantly larger maximum and total void size.

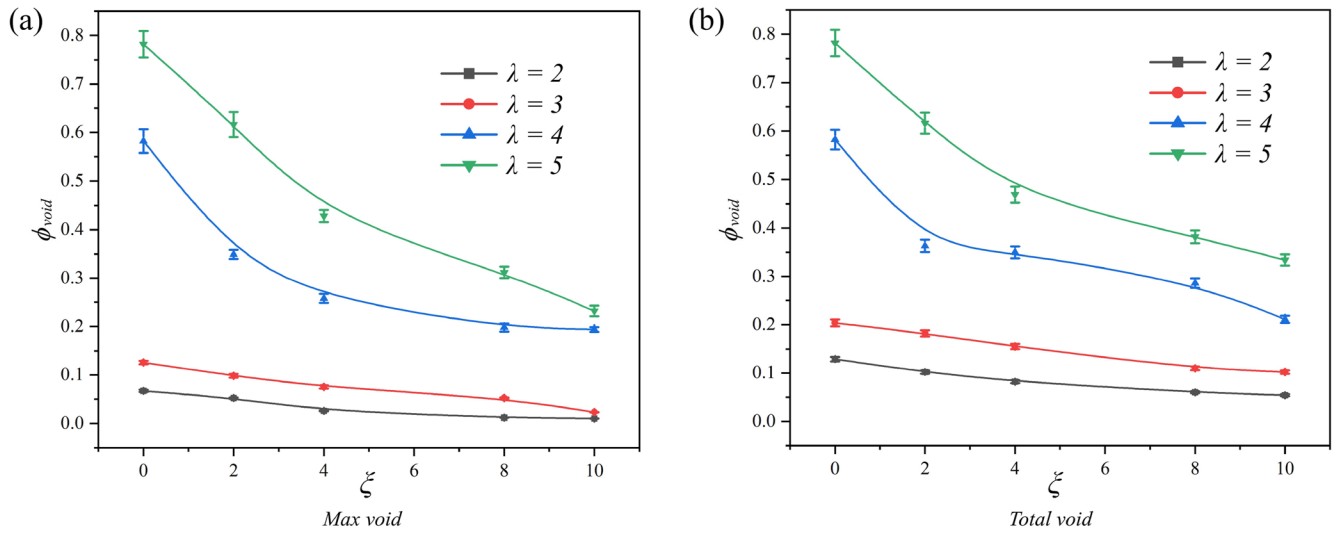

FIG. 5. Statistical summary diagram of (a) the maximum void volume fraction and (b) the total void volume fraction across the parameter (ξ-λ) space.

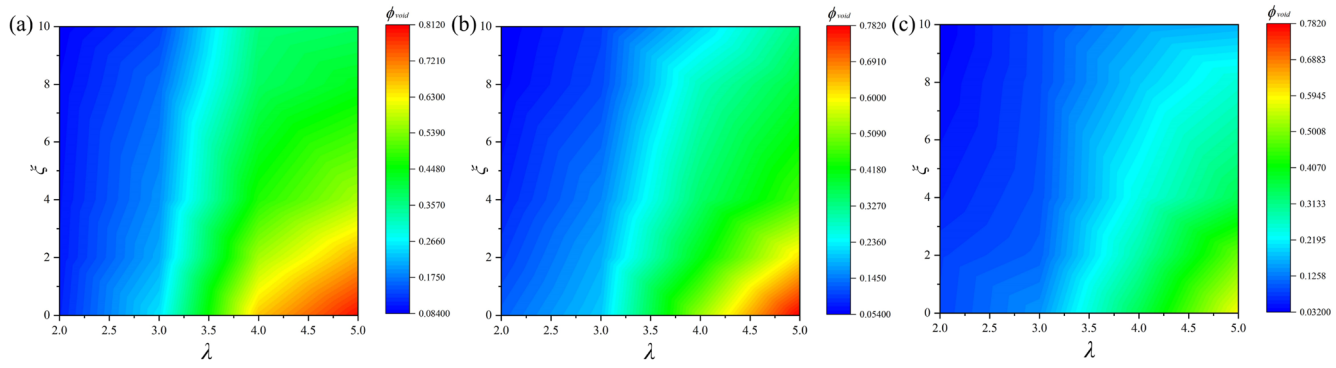

FIG. 6. Global picture of the statistical total void volume fraction across the two-dimensional parameter (ξ-λ) space at (a) $T = 0.8$, (b) $T = 1.0$, and (c) $T = 1.5$.

This observation suggests that the sparsity of the sticker distribution facilitates an enhanced degree of phase separation in the IDP components.

However, when the average interspacing of distribution is relatively small, the variance (the non-uniformity of the arrangement) exerts a negligible influence on the phase separation behavior. In stark contrast, a pronounced alteration in the sticker distribution is evident when the average interspacing is large. Evidently, under the sparse sticker distribution, the non-uniformity in the distribution imposes a significant constraint on the formation of large voids. Only under conditions of diminished variance, indicating a nearly homogeneous arrangement of stickers, does the system demonstrate an augmented tendency toward the generation of extensive voids, concurrently facilitating the emergence of pronounced cluster formations. This discovery provides the additional validation of the trends delineated in Fig. 3. Primarily attributable to the dense configuration of stickers on IDPs, numerous small clusters are dispersed throughout the system—precluding the formation of large, robust aggregations—and ultimately leading to a significant reduction in the system's void volume fraction, a direct consequence of non-uniform sticker distribution. This observation finds strong support in experimental data from Wu *et al.*,[57] who used single-fluorogen tracking and super-resolution imaging to visualize nanoscale spatial inhomogeneity in A1-LCD condensates: specifically, the coexistence of small, slow-moving hubs (formed by reversible cross-linking of aromatic stickers) and fast-dispersed molecules. Their experimental characterization resonates with the core trend of our simulation—namely, that sticker patterning is a key regulator of cluster heterogeneity, as dense sticker configurations similarly favor dispersed small clusters over large aggregations, aligning with our measured reduction in void volume fraction.

Furthermore, to provide a comprehensive overview that elucidates the parameter space conducive to phase separation, we generated a global picture illustrating the two-dimensional parameters at three distinct temperatures, as depicted in Fig. 6. This figure distinctly illustrates that significant void occupation is observed only when stickers are distributed with both large spacing and high uniformity across all three temperatures. Smaller distribution spacing and greater patterning heterogeneity inhibit the formation of large voids, indicating that they hinder the development of large, dense clusters within the system. This observation underscores that robust clustering predominantly occurs in IDPs characterized by a sparse and uniform distribution of stickers, whereas a dense distribution of stickers directly fosters the formation of small, dispersed clusters. In particular, published experimental studies[45,55,58] on model IDPs (e.g., FUS, hnRNPA1, and LAF-1 RGG domains) and related biophysical assays collectively indicate that modulating the spatial distribution of sticker residues (arginine/tyrosine) alters IDP phase separation propensity, with uniformly dispersed stickers favoring the formation of more stable condensates; these overall experimental trends are broadly consistent with the clustering behavior predicted by our simulations. The results are in full agreement with the aforementioned discussion, further corroborating the observed trends.

CONCLUSIONS

In summary, our systematic investigation employing the stickers-and-spacers model has unraveled how coarse-grained sequence patterning in IDPs governs their phase separation behavior. Strikingly, our systematic analysis reveals that the compactness of sticker alignment on IDPs exerts a pronounced regulatory influence on the clustering of phase-separated aggregations, while the heterogeneity in arrangement spacing periodicity further alters the morphology of the resulting cluster assemblies. Further investigations reveal that robust clustering emerges predominantly in systems within IDPs exhibiting sparse and homogeneous sticker distribution, whereas densely packed sticker configurations promote fragmented, spatially dispersed cluster formation. These conclusions are strongly supported by the statistical quantification of the void volume fraction (serving as a referential measure for condensate maturation), complemented with the meticulous quantification of the total stickers present on the cluster surfaces. These results may establish mechanistic principles for modulating IDP-governed phase separation, directly linking its regulation to therapeutic strategies targeting neurodegenerative diseases driven by pathogenic IDP aggregation.

ACKNOWLEDGMENTS

This work was supported by the MOST-NSFC (Grant Nos. 2022YFA1303100 and 32090040) and the Strategic Priority

Research Program of the Chinese Academy of Sciences (Grant No. XDB0450402).

AUTHOR DECLARATIONS

Conflict of Interest

The authors have no conflicts to disclose.

Author Contributions

Xubiao Ji: Conceptualization (equal); Data curation (lead); Formal analysis (lead); Investigation (lead); Methodology (lead); Project administration (supporting); Software (lead); Validation (lead); Visualization (lead); Writing – original draft (lead); Writing – review & editing (equal). **Zhonghuai Hou**: Conceptualization (equal); Data curation (supporting); Formal analysis (supporting); Funding acquisition (lead); Investigation (supporting); Methodology (equal); Project administration (lead); Resources (lead); Software (supporting); Supervision (lead); Validation (supporting); Visualization (supporting); Writing – original draft (supporting); Writing – review & editing (equal).

DATA AVAILABILITY

The data that support the findings of this study are available from the corresponding author upon reasonable request.

REFERENCES

[1]Y. Shin and C. P. Brangwynne, "Liquid phase condensation in cell physiology and disease," Science **357**(6357), eaaf4382 (2017).
[2]S. Ray, N. Singh, R. Kumar, K. Patel, S. Pandey, D. Datta, J. Mahato, R. Panigrahi, A. Navalkar, S. Mehra *et al.*, "α-synuclein aggregation nucleates through liquid-liquid phase separation," Nat. Chem. **12**(8), 705–716 (2020).
[3]M. Feric, N. Vaidya, T. S. Harmon, D. M. Mitrea, L. Zhu, T. M. Richardson, R. W. Kriwacki, R. V. Pappu, and C. P. Brangwynne, "Coexisting liquid phases underlie nucleolar subcompartments," Cell **165**(7), 1686–1697 (2016).
[4]A. G. Larson, D. Elnatan, M. M. Keenen, M. J. Trnka, J. B. Johnston, A. L. Burlingame, D. A. Agard, S. Redding, and G. J. Narlikar, "Liquid droplet formation by HP1α suggests a role for phase separation in heterochromatin," Nature **547**(7662), 236–240 (2017).
[5]M. Farag, S. R. Cohen, W. M. Borcherds, A. Bremer, T. Mittag, and R. V. Pappu, "Condensates formed by prion-like low-complexity domains have small-world network structures and interfaces defined by expanded conformations," Nat. Commun. **13**(1), 7722 (2022).
[6]J. M. Choi, F. Dar, and R. V. Pappu, "LASSI: A lattice model for simulating phase transitions of multivalent proteins," PLoS Comput. Biol. **15**(10), e1007028 (2019).
[7]S. Alberti, A. Gladfelter, and T. Mittag, "Considerations and challenges in studying liquid-liquid phase separation and biomolecular condensates," Cell **176**(3), 419–434 (2019).
[8]C. M. Caragine, S. C. Haley, and A. Zidovska, "Nucleolar dynamics and interactions with nucleoplasm in living cells," eLife **8**, e47533 (2019).
[9]I. A. Sawyer, D. Sturgill, M. H. Sung, G. L. Hager, and M. Dundr, "Cajal body function in genome organization and transcriptome diversity," Bioessays **38**(12), 1197–1208 (2016).
[10]J. E. Henninger, O. Oksuz, K. Shrinivas, I. Sagi, G. LeRoy, M. M. Zheng, J. O. Andrews, A. V. Zamudio, C. Lazaris, N. M. Hannett *et al.*, "RNA-mediated feedback control of transcriptional condensates," Cell **184**(1), 207–225.e24 (2021).
[11]D. Hnisz, K. Shrinivas, R. A. Young, A. K. Chakraborty, and P. A. Sharp, "A phase separation model for transcriptional control," Cell **169**(1), 13–23 (2017).
[12]A. Khong, T. Matheny, S. Jain, S. F. Mitchell, J. R. Wheeler, and R. Parker, "The stress granule transcriptome reveals principles of mRNA accumulation in stress granules," Mol. Cell **68**(4), 808–820.e5 (2017).
[13]J. Guillén-Boixet, A. Kopach, A. S. Holehouse, S. Wittmann, M. Jahnel, R. Schlüßler, K. Kim, I. R. E. A. Trussina, J. Wang, D. Mateju *et al.*, "RNA-induced conformational switching and clustering of G3BP drive stress granule assembly by condensation," Cell **181**(2), 346–361.e17 (2020).
[14]L. B. Case, X. Zhang, J. A. Ditlev, and M. K. Rosen, "Stoichiometry controls activity of phase-separated clusters of actin signaling proteins," Science **363**(6431), 1093–1097 (2019).
[15]S. F. Banani, H. O. Lee, A. A. Hyman, and M. K. Rosen, "Biomolecular condensates: Organizers of cellular biochemistry," Nat. Rev. Mol. Cell Biol. **18**(5), 285–298 (2017).
[16]S. Saha, C. A. Weber, M. Nousch, O. Adame-Arana, C. Hoege, M. Y. Hein, E. Osborne-Nishimura, J. Mahamid, M. Jahnel, L. Jawerth *et al.*, "Polar positioning of phase-separated liquid compartments in cells regulated by an mRNA competition mechanism," Cell **166**(6), 1572–1584.e16 (2016).
[17]C. P. Brangwynne, C. R. Eckmann, D. S. Courson, A. Rybarska, C. Hoege, J. Gharakhani, F. Jülicher, and A. A. Hyman, "Germline P granules are liquid droplets that localize by controlled dissolution/condensation," Science **324**(5935), 1729–1732 (2009).
[18]C. Wang, Y. Duan, G. Duan, Q. Wang, K. Zhang, X. Deng, B. Qian, J. Gu, Z. Ma, S. Zhang *et al.*, "Stress induces dynamic, cytotoxicity-antagonizing TDP-43 nuclear bodies via paraspeckle LncRNA NEAT1-mediated liquid-liquid phase separation," Mol. Cell **79**(3), 443–458.e7 (2020).
[19]R. K. Das, K. M. Ruff, and R. V. Pappu, "Relating sequence encoded information to form and function of intrinsically disordered proteins," Curr. Opin. Struct. Biol. **32**, 102–112 (2015).
[20]J. D. Forman-Kay and T. Mittag, "From sequence and forces to structure, function, and evolution of intrinsically disordered proteins," Structure **21**(9), 1492–1499 (2013).
[21]V. N. Uversky, "Intrinsically disordered proteins in overcrowded milieu: Membrane-less organelles, phase separation, and intrinsic disorder," Curr. Opin. Struct. Biol. **44**, 18–30 (2017).
[22]J. McCarty, K. T. Delaney, S. P. O. Danielsen, G. H. Fredrickson, and J. E. Shea, "Complete phase diagram for liquid-liquid phase separation of intrinsically disordered proteins," J. Phys. Chem. Lett. **10**(8), 1644–1652 (2019).
[23]A. Bah, R. M. Vernon, Z. Siddiqui, M. Krzeminski, R. Muhandiram, C. Zhao, N. Sonenberg, L. E. Kay, and J. D. Forman-Kay, "Folding of an intrinsically disordered protein by phosphorylation as a regulatory switch," Nature **519**(7541), 106–109 (2015).
[24]T. S. Harmon, A. S. Holehouse, M. K. Rosen, and R. V. Pappu, "Intrinsically disordered linkers determine the interplay between phase separation and gelation in multivalent proteins," eLife **6**, e30294 (2017).
[25]A. Majumdar, P. Dogra, S. Maity, and S. Mukhopadhyay, "Liquid-liquid phase separation is driven by large-scale conformational unwinding and fluctuations of intrinsically disordered protein molecules," J. Phys. Chem. Lett. **10**(14), 3929–3936 (2019).
[26]A. Garaizar, I. Sanchez-Burgos, R. Collepardo-Guevara, and J. R. Espinosa, "Expansion of intrinsically disordered proteins increases the range of stability of liquid-liquid phase separation," Molecules **25**(20), 4705 (2020).
[27]G. L. Dignon, W. Zheng, R. B. Best, Y. C. Kim, and J. Mittal, "Relation between single-molecule properties and phase behavior of intrinsically disordered proteins," Proc. Natl. Acad. Sci. U. S. A. **115**(40), 9929–9934 (2018).
[28]C. B. Anfinsen, "Principles that govern the folding of protein chains," Science **181**(4096), 223–230 (1973).
[29]V. N. Uversky, "Under-folded proteins: Conformational ensembles and their roles in protein folding, function, and pathogenesis," Biopolymers **99**(11), 870–887 (2013).
[30]K. H. DuBay, G. R. Bowman, and P. L. Geissler, "Fluctuations within folded proteins: Implications for thermodynamic and allosteric regulation," Acc. Chem. Res. **48**(4), 1098–1105 (2015).
[31]H. J. Dyson and P. E. Wright, "Intrinsically unstructured proteins and their functions," Nat. Rev. Mol. Cell Biol. **6**(3), 197–208 (2005).

[32]V. N. Uversky, J. R. Gillespie, and A. L. Fink, "Why are 'natively unfolded' proteins unstructured under physiologic conditions?," Proteins **41**(3), 415–427 (2000).
[33]P. Tompa, "Intrinsically disordered proteins: A 10-year recap," Trends Biochem. Sci. **37**(12), 509–516 (2012).
[34]C. J. Oldfield and A. K. Dunker, "Intrinsically disordered proteins and intrinsically disordered protein regions," Annu. Rev. Biochem. **83**, 553–584 (2014).
[35]E. W. Martin, A. S. Holehouse, C. R. Grace, A. Hughes, R. V. Pappu, and T. Mittag, "Sequence determinants of the conformational properties of an intrinsically disordered protein prior to and upon multisite phosphorylation," J. Am. Chem. Soc. **138**(47), 15323–15335 (2016).
[36]Y. Wang, J. C. Fisher, R. Mathew, L. Ou, S. Otieno, J. Sublet, L. Xiao, J. Chen, M. F. Roussel, and R. W. Kriwacki, "Intrinsic disorder mediates the diverse regulatory functions of the Cdk inhibitor p21," Nat. Chem. Biol. **7**(4), 214–221 (2011).
[37]P. E. Wright and H. J. Dyson, "Intrinsically unstructured proteins: Re-assessing the protein structure-function paradigm," J. Mol. Biol. **293**(2), 321–331 (1999).
[38]A. S. Holehouse and B. B. Kragelund, "The molecular basis for cellular function of intrinsically disordered protein regions," Nat. Rev. Mol. Cell Biol. **25**(3), 187–211 (2024).
[39]B. A. Gibson, L. K. Doolittle, M. W. G. Schneider, L. E. Jensen, N. Gamarra, L. Henry, D. W. Gerlich, S. Redding, and M. K. Rosen, "Organization of chromatin by intrinsic and regulated phase separation," Cell **179**(2), 470–484.e21 (2019).
[40]F. X. Theillet, A. Binolfi, B. Bekei, A. Martorana, H. M. Rose, M. Stuiver, S. Verzini, D. Lorenz, M. van Rossum, D. Goldfarb, and P. Selenko, "Structural disorder of monomeric α-synuclein persists in mammalian cells," Nature **530**(7588), 45–50 (2016).
[41]K. H. Utami, S. Morimoto, Y. Mitsukura, and H. Okano, "The roles of intrinsically disordered proteins in neurodegeneration," Biochim. Biophys. Acta, Gen. Subj. **1869**(4), 130772 (2025).
[42]A. Patel, H. O. Lee, L. Jawerth, S. Maharana, M. Jahnel, M. Y. Hein, S. Stoynov, J. Mahamid, S. Saha, T. M. Franzmann *et al.*, "A liquid-to-solid phase transition of the ALS protein FUS accelerated by disease mutation," Cell **162**(5), 1066–1077 (2015).
[43]J. M. Choi, A. S. Holehouse, and R. V. Pappu, "Physical principles underlying the complex biology of intracellular phase transitions," Annu. Rev. Biophys. **49**, 107–133 (2020).
[44]A. Bremer, M. Farag, W. M. Borcherds, I. Peran, E. W. Martin, R. V. Pappu, and T. Mittag, "Deciphering how naturally occurring sequence features impact the phase behaviours of disordered prion-like domains," Nat. Chem. **14**(2), 196–207 (2022).
[45]E. W. Martin, A. S. Holehouse, I. Peran, M. Farag, J. J. Incicco, A. Bremer, C. R. Grace, A. Soranno, R. V. Pappu, and T. Mittag, "Valence and patterning of aromatic residues determine the phase behavior of prion-like domains," Science **367**(6478), 694–699 (2020).
[46]X. Zeng, C. Liu, M. J. Fossat, P. Ren, A. Chilkoti, and R. V. Pappu, "Design of intrinsically disordered proteins that undergo phase transitions with lower critical solution temperatures," APL Mater. **9**(2), 021119 (2021).
[47]M. Rubinstein and A. N. Semenov, "Dynamics of entangled solutions of associating polymers," Macromolecules **34**(4), 1058–1068 (2001).
[48]A. N. Semenov and M. Rubinstein, "Thermoreversible gelation in solutions of associative polymers. 1. Statics," Macromolecules **31**(4), 1373–1385 (1998).
[49]I. Alshareedah, M. M. Moosa, M. Pham, D. A. Potoyan, and P. R. Banerjee, "Programmable viscoelasticity in protein-RNA condensates with disordered sticker-spacer polypeptides," Nat. Commun. **12**(1), 6620 (2021).
[50]G. M. Ginell and A. S. Holehouse, "An introduction to the stickers-and-spacers framework as applied to biomolecular condensates," Methods Mol. Biol. **2563**, 95–116 (2023).
[51]S. Ranganathan and E. I. Shakhnovich, "Dynamic metastable long-living droplets formed by sticker-spacer proteins," eLife **9**, e56159 (2020).
[52]H. Jiang, S. Wang, Y. Huang, X. He, H. Cui, X. Zhu, and Y. Zheng, "Phase transition of spindle-associated protein regulate spindle apparatus assembly," Cell **163**(1), 108–122 (2015).
[53]T. J. Nott, E. Petsalaki, P. Farber, D. Jervis, E. Fussner, A. Plochowietz, T. D. Craggs, D. P. Bazett-Jones, T. Pawson, J. D. Forman-Kay, and A. Baldwin, "Phase transition of a disordered nuage protein generates environmentally responsive membraneless organelles," Mol. Cell **57**(5), 936–947 (2015).
[54]S. Xiang, M. Kato, L. C. Wu, Y. Lin, M. Ding, Y. Zhang, Y. Yu, and S. L. McKnight, "The LC domain of hnRNPA2 adopts similar conformations in hydrogel polymers, liquid-like droplets, and nuclei," Cell **163**(4), 829–839 (2015).
[55]J. Wang, J. M. Choi, A. S. Holehouse, H. O. Lee, X. Zhang, M. Jahnel, S. Maharana, R. Lemaitre, A. Pozniakovsky, D. Drechsel *et al.*, "A molecular grammar governing the driving forces for phase separation of prion-like RNA binding proteins," Cell **174**(3), 688–699.e16 (2018).
[56]K. M. Ruff, T. S. Harmon, and R. V. Pappu, "CAMELOT: A machine learning approach for coarse-grained simulations of aggregation of block-copolymeric protein sequences," J. Chem. Phys. **143**(24), 243123 (2015).
[57]T. Wu, M. R. King, Y. Qiu, M. Farag, R. V. Pappu, and M. D. Lew, "Single fluorogen imaging reveals distinct environmental and structural features of biomolecular condensates," Nat. Phys. **21**(5), 778–786 (2025).
[58]B. S. Schuster, G. L. Dignon, W. S. Tang, F. M. Kelley, A. K. Ranganath, C. N. Jahnke, A. G. Simpkins, R. M. Regy, D. A. Hammer, M. C. Good, and J. Mittal, "Identifying sequence perturbations to an intrinsically disordered protein that determine its phase-separation behavior," Proc. Natl. Acad. Sci. U. S. A. **117**(21), 11421–11431 (2020).